INVESTIGATION OF THE CORE OF EXTENSIVE AIR SHOWERS

S. N. VERNOV, N. N. GORYUNOV, G. T. ZATSEPIN, G. V. KULINKOV, Yu. A. NECHIN, Z. S. STRUGALSKIĬ, and G. B. KHRISTIANSEN

Moscow State University

P. N. Lebedev Physics Institute, Academy of Sciences, U.S.S.R.

Submitted to JETP editor July 21, 1958

J. Exptl. Theoret. Phys. (U.S.S.R.) **36**, 669-681 (March, 1959)

A new method of investigation of individual air showers is described. The method is applied to the study of the core of extensive air showers. Some preliminary experimental data, indicating the existence of large fluctuations of the energy flux of the electron-photon and of the nuclear-active components in the core of extensive air showers are presented.

THE necessity of studying individual extensive air showers (EAS) simultaneously at different depths was recently pointed out by D. V. Skobel'tsyn. The present work is an attempt to carry out this idea in connection with the study of the core of EAS.

A detailed study of EAS, carried out in recent years in a series of experiments,[1-4] showed that the lateral distribution of particles in EAS does not vary at different altitudes of the atmosphere and, at any given altitude is, as a whole, described by the electromagnetic cascade theory in the central regions of the shower up to small distances of ~ 1 m from the shower axis. An analysis of the data pointed to the conclusion that a nuclear cascade is present in the shower, and that the main part of the energy flux of the nuclear cascade should be concentrated at small distances from the axis (~ 1 m), forming the so-called core of the EAS.[5]

The study of the core region of EAS therefore becomes of special interest, since, in that region, one can observe the specific features of the nuclear-cascade process. In connection with the above, an array for a detailed study of the core of the EAS was constructed. The array for the study of the core of the EAS, which forms a part of the large array set up at Moscow State University for a comprehensive study of EAS, is described below, and preliminary results of measurements, illustrating the method used, are presented. A full report on the experimental results and their analysis will be given in future articles.

DESCRIPTION OF THE ARRAY

The array makes it possible to obtain detailed data on the electron-photon and nuclear-active components in the core of the EAS. A block diagram of the array is presented in Figs. 1a and 1b. The array consists of a diffusion chamber with an area of 0.64 m^2, 124 ionization chambers displayed on a hodoscope and screened by a special absorber, and 672 hodoscope Geiger-Müller counters of various sizes.

A picture of the distribution of the shower-particle flux (mainly electrons) is obtained near the shower axis by means of the diffusion chamber and of the hodoscope counters. This data can be used to determine the number of particles in the shower and also the position of its axis, by means of the well-known method.[2,6] This can be done to an accuracy of ~ 1 m using the hodoscope-counter data, and to an accuracy of a few centimeters if the axis falls within the diffusion chamber. It is also evident that the diffusion chamber gives a full picture of the directions of single shower particles, and therefore makes it possible to determine the direction of the particle flux near the shower axis.

The distribution of the energy flux carried by the electron-photon component near the shower axis was determined by means of the first row of ionization chambers, consisting of 60 cubic chambers with the dimensions $25 \times 25 \times 25$ cm and screened from above by 2.5 cm of lead. In fact, the multiplication coefficient for such a thickness of lead is, with sufficient accuracy, proportional to the mean energy of the particles (electrons and photons) at a given distance from the shower axis, if the energy lies in the range 10^8 to 10^{11} ev. A direct inspection of the distribution of the flux in the first row of ionization chambers makes it possible to determine the position of the shower axis with an accuracy of the same order of magnitude as the dimensions of the chambers.

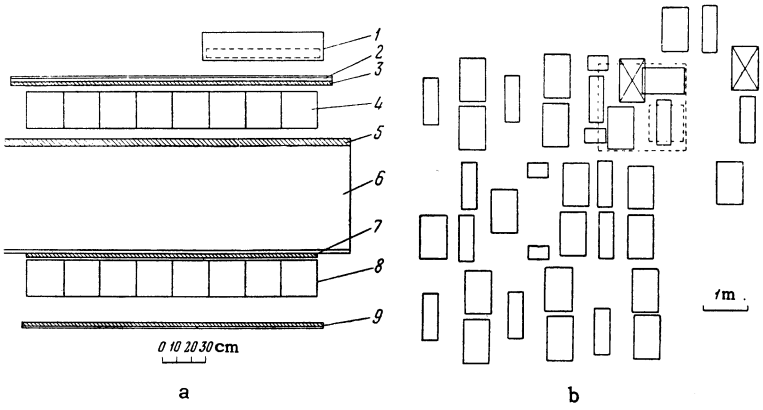

FIG. 1a. Position of the diffusion chamber, ionization chambers and layers of the absorbers. 1 – diffusion chamber (the sensitive region is shown by the dashed line); 2 – Al, 0.3 cm; 3 – Pb, 2.5 cm (28.2 g/cm²); 4 – ionization chambers; 5 – Pb, 5 cm; 6 – graphite, 73 cm (120 g/cm²); 7 – Pb, 2.5 cm; 8 – ionization chambers; 9 – Pb, 2 cm; between the layers 2–3 and 6–7 – wood, 2.5 cm; between 3–4 and 7–8 – plywood, 0.4 cm.

FIG. 1b. Position of ionization chambers, diffusion chambers (shown by dotted line), and Geiger-Müller counters. Large rectangles – effective areas of trays consisting of 12 counters 330 cm² each; middle sized rectangles – 24 counters 100 cm² each; small rectangles – 24 cm² each. The counters in the trays are placed at the distance of half a diameter one from another. The trays denoted by a cross contain a group of counters connected to a six-fold coincidence circuit. The plane of the counters is at a distance of 1.15 m from the first row of ionization chambers 4.

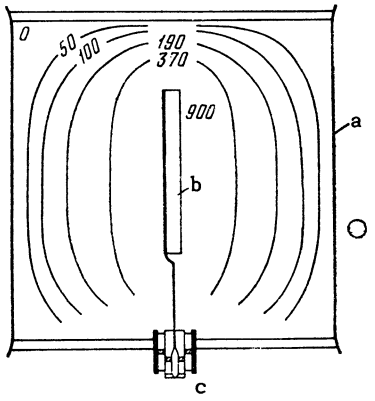

FIG. 2. Cross section of the ionization chamber, a – walls; b – collecting electrode; c – insulator.

The distribution of the energy flux carried by the nuclear-active component in the shower core can be determined by means of the second row, consisting of 64 ionization chambers placed under a composite of 7.5 cm lead, 70 cm of graphite (120 g/cm²), and 2.5 cm of lead. The electron-photon component of the shower coming from the air is almost entirely absorbed, and thus does not reach the lower row of chambers.

Nuclear-active particles incident upon the absorber initiate a nuclear cascade inside it. In each nuclear collision, part of the energy is irreversibly transferred to photons through production and consecutive decay of π^0 mesons. The thickness of the layer of lead placed above the graphite amounts to half of the mean free path of nuclear-active particles, and the thickness of the graphite to 1.7 of the mean free path. Therefore, the energy transfer from nuclear-active particles to photons occurs mainly in graphite, in which the energy is accumulated, since electron-photon cascades develop weakly in graphite. The graphite therefore acts as a singular transformer of the energy of the nuclear-active particles into the energy of the electron-photon component. The development of the electron-photon cascade occurs mainly in the lower layer of lead, and, after it has traversed this layer, the cascade reaches approximately its maximum. The number of electrons falling on the lower chambers is thus proportional to the energy transferred to π^0 mesons in graphite and consequently, on the average, to the energy of the primary nuclear-active particle. The efficiency of such a method for recording of high-energy nuclear-active particles was discussed earlier,[7] and this method was used by Dmitriev, Kulikov, and Khristiansen.[8] The values of energy E_{n-a} of the nuclear-active component as listed below, are calculated from the relation[9]

$$E_{n-a} = 5 \cdot 10^8 n \text{ ev},$$

where n is the number of relativistic particles recorded in the lowest row of chambers.

It can be seen from Fig. 1a that the diffusion chamber is screened from below by 3 mm of Al from the electrons and photons scattered by the lead. The ionization chambers of the first and second rows are so to speak in a lead gap, since they are screened by lead also from below. This makes it possible to interpret the experimental data using the cascade theory for heavy elements without any limitations (accounting only for corrections due to the absorption in the walls of the chambers). In calculating the value of the energy flux E of the electron-photon component incident upon the chamber, it was assumed, following Ivanenko,[10] that

$$E = 10^8 n' \text{ ev},$$

where n′ is the number of relativistic particles recorded in the chamber.

The diffusion chamber used in the array measures 800×800×60 mm, where 60 mm is the height of the sensitive layer. The bottom of the chamber is kept at −50°C, and is maintained constant within ±1°, across the area of the bottom and also with respect to time, by means of a special two-stage compression freon refrigerating system. The lid of the chamber is kept at +20°C. The chamber is filled with alcohol vapor. A grid is placed above the sensitive volume and kept at a potential of −40 v with respect to the bottom of the chamber. The use of such an electric field leads to a decrease of the duration of tracks, and considerably lowers the background, which amounts to 50 tracks per grid unit. The sensitive layer is illuminated through a yellow filter by means of pulsed lamps ITS-1500, which are triggered by the master pulse. The sensitive layer is photographed by a stereoscopic camera with 72 mm base through the glass lid of the chamber of 1.5 g/cm^2 thickness.

The block of ionization chambers consists of 124 cubic chambers 25×25×25 cm. Each of the chambers is connected to its own channel of the electronic recording system for the pulse amplitudes. The ionization chambers are filled with a mixture of spectrally pure argon (98%), and chemically pure nitrogen (2%) to the pressure of 830 mm Hg, with preliminary evacuation (and simultaneous heating) to 10^{-4} mm Hg. The cross section of the chamber is shown in Fig. 2.* The walls of the chambers are made of stainless steel 2 mm thick, with the exception of the top wall which is 1 mm thick. The collection electrode is cylindrical in shape, 10 mm in diameter and 100 mm long. A cross section through the equipotential surfaces, for a potential difference between the collecting electrode and the walls equal to 900 v which corresponds to the chosen working voltage† is shown in Fig. 2. The picture of the equipotential surfaces was obtained by the electrolytic-tank method as used by Goryunov and Erlykin.[11] From this picture we can determine the velocity of collection of electrons for local ionization in various places of the chamber. For a uniform volume ionization, the velocity of collection of electrons is such that, within 2×10^{-5} sec, the pulse attains 80% of its amplitude.

*For convenience and speed of filling, the ionization chambers were built as blocks of four chambers with a single outlet for filling.

†The saturation of the electron current in the chamber, for volume ionization equivalent to the passage of 10 000 relativistic particles during the collection time of 20 μsec, produced by a preparate of Co^{60}, occurs at a potential difference of 300 v.

Our basic demands of the electronic circuits are: a possibility of recording pulses with a wide range of amplitudes, and stability of operation. In the experiment, the pulse amplitudes of the ionization chambers are recorded as following: (For a more detailed description see reference 12): A preamplifier with an amplification factor of ~100 is attached to each chamber. The pulse was transmitted by a cathode follower through a cable to a nonlinear amplifier, and then to a switching tube. Whenever this tube receives the master pulse simultaneously, the amplified pulse of the chamber is fed to a storage circuit, and is then collected by means of an electronic switch which serves all 124 chambers. The pulse arrives at the vertical deflection plates of a CRO tube, delayed with respect to the master pulse that triggers the time base by an amount different for each channel. The total picture of the distribution of pulse amplitudes in all ionization chambers is recorded photographically. By means of the setup described, it is possible to record pulses produced by the passage of 5 to 40,000 relativistic particles through the chamber. The lower limit is determined by the amplifier noise and especially that in the pre-amplifier. Evidently, the introduction of a non-linear amplifier, which makes a wider dynamical range possible, leads to a worse accuracy in the determination of the pulse heights. However, for 85% of the range, the accuracy is not worse from 10%, and for 15% of the range it amounts to ~25%.

The chambers were calibrated by photographing pulses from single relativistic particles traversing the volume of the chamber. The pulse on the grid of the first tube of the pre-amplifier, produced by the passage of a single relativistic particle through the chamber, amounts to ~20 μv.

The comparatively low frequency of the observed events, and the ensuing long time needed for measurements makes a systematic check of the operation of the whole electronic system and of the ionization chamber a necessity. All amplifiers and recording channels were calibrated regularly every 24 hours. To this end, pulses of given amplitude from a pulse generator were fed simultaneously through a small capacity to the grids of the first tubes of all pre-amplifiers. From the obtained photographs of calibration pulses of various amplitudes, amplitude characteristics of the separate channels were constructed, and these are used for evaluating the oscillograms. One example of such amplitude characteristics is shown in Fig. 3. Tests showed that the amplitude characteristics did not change substantially during a long period of operation. By means of the above method of calibration, one can check the

amplifying-recording chain as a whole, including the input capacity of the pre-amplifier. The condition of the gas in the chambers which was not checked in the above-described procedure, was tested periodically once very half year. The chambers were irradiated by γ-rays from a Co^{60} source in a fixed geometry, and the value of fluctuations of the electron current in the chamber was measured.

The hodoscope consists of 264 counters with an area 330 cm^2 each, 312 counters with an area of 100 cm^2, and 96 counters with an area of 24 cm^2 each. All counters were connected to HK-7 hodoscope circuits using cold thyratrons of type MTK-90. The average resolving time of the circuit is 15 μsec.

The whole array is triggered by pulses produced whenever an EAS passes through the array, and also when large bursts are produced in the blocks of ionization chambers. The selection of EAS is determined by the requirement of a simultaneous discharge of six groups of counters with an area of 0.132 m^2 each, from those placed 1 m above the first row of ionization chambers. Such a method of selection makes it possible to record showers with a number of particles $N \gtrsim 10^4$, and with axes that are incident, on the average, at a distance of several tens of meters from the array.

The bursts are selected in the following way: The sum of the amplitude of the pulses from all 124 chambers should correspond to the ionization produced in the working volume of the chambers by a vertical flux of 1000 relativistic particles. Such an ionization can be produced by (1) a flux of EAS particles with an axis close to the array, (2) by high-energy nuclear-active particles, (3) by radiation showers from high-energy μ mesons, and (4) by nuclear disintegrations in the gas and in the walls of the chambers. The greater fraction of the bursts selected by the master-system are connected with the passage of EAS and, in their number, showers of comparatively low density whose cores contain high-energy nuclear-active particles. We note that the fourth cause listed above is not significant in view of the following properties of the selection system: The addition of the pulses of the chambers takes place after their nonlinear amplification. For the production of the masterpulse, it is necessary that the amplitude of the total pulse is bigger than a certain value (see Fig. 3, point A). Because of the nonlinearity, it is clear that the required amplitude of the pulse can be reached when several chambers each produce a smaller total burst than that due to a single chamber. When the total ionization is distributed among two or more chambers so that in one of them the observed ionization amounts to not more than half of the total, then the threshold corresponds to 1000 relativistic particles. For ionization in one of the chambers only, the threshold corresponds to 4000 relativistic particles. Nuclear disintegrations thus lead to the production of a master pulse only when the produced ionization is bigger than 4000 relativistic particles.

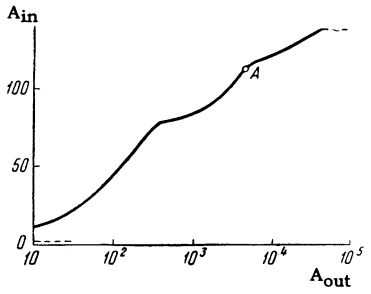

FIG. 3. Amplitude characteristics of one of the channels of nonlinear amplification. The x axis represents the value of ionization in number of relativistic particles, the y axis – the amplitude in mm of the vertical deflection on the CRO tube.

At the same time, bursts produced by nuclear-active particles and μ mesons will cause the appearance of a master pulse with 100% probability if the ionization produced by them is bigger than 1300 relativistic particles since, in that case, at least 10% of the ionization will be produced in adjoining chambers in view of the wide angular distribution of particles of the electron-photon showers in lead. Radiation showers from μ mesons (the third cause) amount to about 20% of all bursts. These bursts are rarely accompanied by shower, and, in the case of μ mesons going close to the horizontal plane, the typical elongation of the burst occurs.

The master pulse from the six-fold coincidence circuit is fed after transformation to switching tubes to the electronic switch and the CRO tube of the block of ionization chambers, to the controls of the flash for the diffusion chamber, and to the master system of the hodoscope HK-7. The flashing of the lamps of the diffusion chamber takes place approximately 0.4 sec after the arrival of the master pulse, which corresponds to the time of growth of the tracks to optimal size. The master pulses are fed to hodoscope circuits with a delay of the order of several μsec, so that they arrive in the middle of the working range of these circuits. The triggering by means of big pulses from the ionization chamber of the two-stage type,[8] which is necessary since the rise time of ionization-chamber pulses is larger than the operation cycle of the hodoscope system. The master pulse is produced every time the total pulse is bigger than the value corresponding to the passage of 300 relativistic particles. However, the hodoscope is photographed

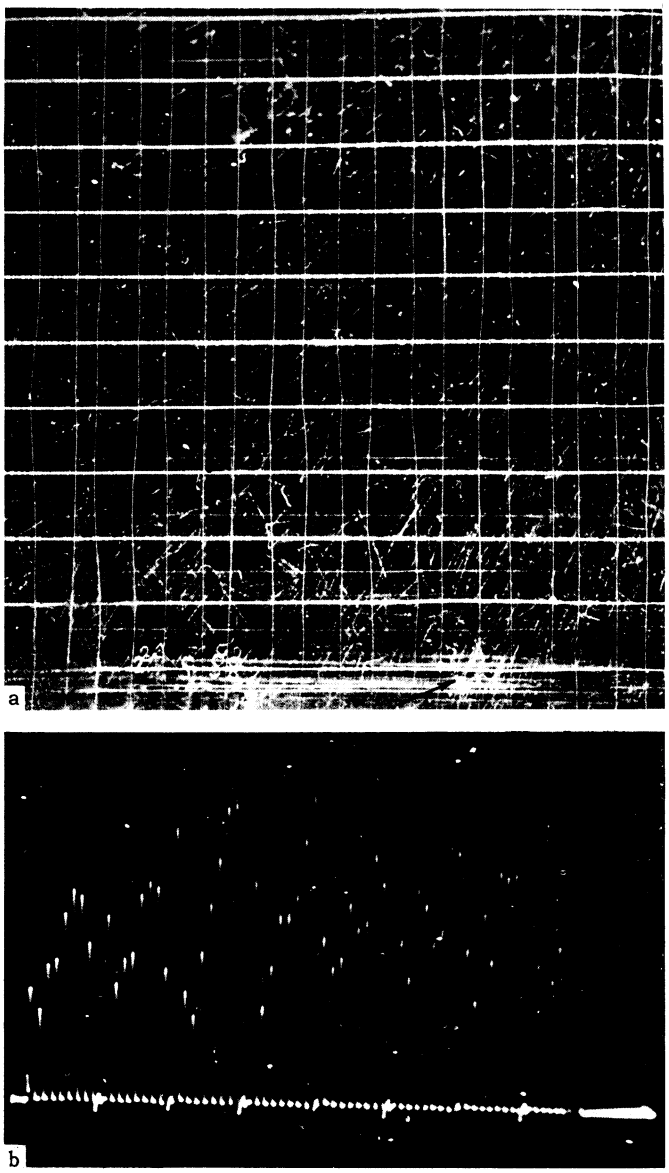

FIG. 4a. A photograph of the diffusion chamber at the moment of passage of an EAS (the arrow indicates the position of the axis.

FIG. 4b. Oscillogram of pulses from 64 ionization chambers during the passage of the core of an EAS through the array.

only when the pulse in the chambers is bigger than 1000 relativistic particles. The dead time of ionization chambers and of hodoscope counters is not greater than 1 sec. The dead time of all elements of the array is not bigger than 10 sec, which makes possible a 90% efficiency of the operation of the array for the chosen frequency of master pulses.

RESULTS AND CERTAIN EXPERIMENTAL PROBLEMS

Up to the present, all elements of the array have been operated for about 1300 hours. During this time, more than 10,000 EAS were recorded. A portion of these events correspond to the incidence of the axes of EAS upon the array. A photograph of the diffusion chamber and an oscillogram of the pulses from ionization chambers corresponding to the arrival of an EAS are shown in Fig. 4.

We shall consider first the densest of the recorded showers. If a shower develops according to the electromagnetic cascade theory, then the axes of high-energy showers may be located within a very small area due to the large density of particle and the presence of high-energy particles which produce a density gradient already at small distances from the axis. For a real shower containing a nuclear cascade, the core of high-energy showers can be studied in greatest detail, since in the development of such showers, a big role is played by nuclear-active particles of energies sufficiently high to concentrate near the axis within a region which is smaller than the dimensions of the array.

When the axis of an EAS passes through the first row of ionization chambers, which records the particles produced as the result of the multiplication of the electrons and photons of the shower in lead, then one can expect an essentially homogeneous distribution of ionization over the whole area occupied by the chambers, together with the presence of a region where the ionization will attain a maximum value.* The axis of the shower can then be determined from the condition that the particle density is maximum at the axis, and is symmetrical about it. We used this method of axis location.

During the 1000 hours of operation of the array, we recorded 28 events interpreted as the passage of EAS with a number of particles $N > 10^5$ through the first row of ionization chambers.†

The number of events observed in which the shower axis fell on the array according to the chosen method of analysis may be compared with

*The difference between a real shower and an electron-photon shower can be observed from the influence, at small distances from axis, of the nuclear scattering of π^0 mesons, producing the electron-photon cascade, as a result of which the axis of the shower may be less sharp than in the case of electron-photon showers. The angular deviation of a photon of energy E from the shower axis amounts to E_s/E. The angle of the π^0 meson in its production is of the order of $\sim \mu_{\pi^0} c^2 / E_{\pi^0}$. Therefore a photon of given energy, produced directly by a π^0 meson, has a larger angle than a similar photon radiated by an electron.

†The position of the axis can be determined without ambiguity if we consider the incidence of axis into a region surrounded by a single external row of ionization chambers. The area of this region is 2.25 m^2. Out of the 28 axes, 15 fell into this region. This number corresponds to the one expected, since the area covered by all chambers amounts to 4 m^2.

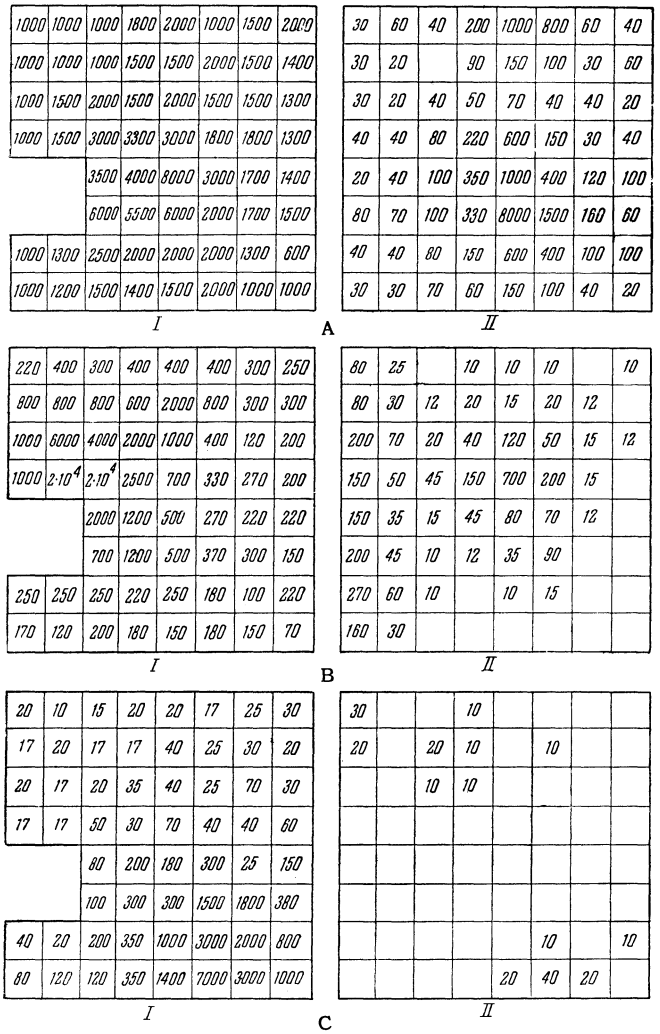

FIG. 5. Distribution of ionization expressed in the number of relativistic particles passing through a chamber, in the first row of ionization chambers (I), and in the second row of ionization chambers (II). A – passage of the shower core with total number of particles $N = 5 \times 10^5$, the lateral distribution of energy flux (first row) $\sim 1/r$; B – $N = 1.3 \times 10^5$, lateral distribution of energy flux $\sim 1/r^2$; C – $N \approx 10^5$, the lateral distribution of energy flux $\sim 1/r^3$.

that which one would expect according to the data on the absolute intensity of showers.[6] According to reference 6, during 1000 hours one would expect 29 axes of showers with a number of particles $N > 10^5$ incident upon the area of 4 m^2, which is in agreement with the data given above.

In all cases, a large gradient of the energy-flux density of the electron-photon component near the axis is observed in the first row of ionization chambers, the degree of which is, however, different for different events. If the gradient is represented by a power law $1/r^k$ for 30 cm < r < 1 m, then the exponent can be within the limits of 1 to 3. The main number of events correspond to values of the exponent $1 < k < 2$. Examples of the observed distribution are shown in Fig. 5.

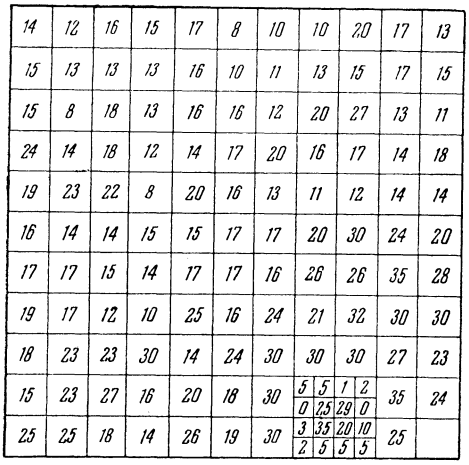

FIG. 6. Distribution of shower particles in the diffusion chamber for an event in which the axis of an EAS with total of particles equal to 2×10^6 passed through the chamber. Total number of shower particles in the chamber – 2308. The number of shower particles is given for cells with an area of 48 cm^2 (12 cm^2 around the axis).

The actual distribution of the energy flux may be steeper since, owing to the large height of the chambers, and the wide angular distribution of particles in lead, the particles from smaller distances may arrive at greater distances from the axis. However, the effect is qualitatively small for the distribution $1/r^k$ for $k < 3$, and for an isotropic distribution of shower particles in lead.

In a number of cases, it was possible to obtain more detailed data on the flux of particles near the core, and on the structure of the shower at still smaller distances from the axis, by means of the diffusion chamber. Out of 28 cases of incidence of the axis of showers on ionization chambers, a marked gradient of particle density is observed in the diffusion chamber for three cases. The distribution of particles in these cases was measured looking at the pictures in a stereoscope. One of these pictures is shown in Fig. 6.

The position of the axis in case of dense showers can be determined from a direct comparison of the particle density in various places in the chamber. The axis of the showers should therefore be found within the limits of such a region where the number of shower particles is larger by an amount greater than the Poisson fluctuation than that in the surrounding adjacent regions of the same dimensions.* The dimensions of this region in the observed three cases were smaller than 5 cm.

The distribution of the particle flux around the shower axis in the diffusion chamber for the observed three cases was found to be $\rho(r) \sim 1/\sqrt{r}$

*Therefore, the accuracy in determining the position of the axis depends essentially on the shower size.

TABLE I

Angle with the axis, ϑ^0	Number of particles in a circle with radius		
	$r = 15$ cm	$r = 30$ cm	$r = 45$ cm
0—2	34(34)	74(54)	74(54)
2—4	62(62)	90(76)	90(76)
4—6	3(3)	25(14)	55(27)
6—8	0(0)	24(12)	46(22)
8—10	0(0)	4(2)	20(10)
10—16	1(1)	8(4)	28(12)

TABLE II

No.	N_s	$E_{e\text{-}p} = N_s 2\beta$ (ev)	$E_{n\text{-}a}$ (ev)	$E_{e\text{-}p}$ in the core (ev)	$\frac{E_{n\text{-}a}}{E_{e\text{-}p}}$	$\frac{E_{e\text{-}p\ core}}{E_{e\text{-}p}}$
1	$5 \cdot 10^5$	$7.2 \cdot 10^{13}$	$9.3 \cdot 10^{12}$	$1.2 \cdot 10^{13}$	0.13	0.17
2	$1.8 \cdot 10^5$	$2.6 \cdot 10^{13}$	$1.3 \cdot 10^{12}$	$1.7 \cdot 10^{12}$	0.049	0.065
3	$2 \cdot 10^5$	$2.9 \cdot 10^{11}$	$4.6 \cdot 10^{11}$	$5.2 \cdot 10^{12}$	0.016	0.18
4	$1.1 \cdot 10^5$	$1.6 \cdot 10^{13}$	$8.5 \cdot 10^{11}$	$8.4 \cdot 10^{11}$	0.053	0.052
5	$2.5 \cdot 10^5$	$3.6 \cdot 10^{13}$	$7 \cdot 10^{11}$	$5.1 \cdot 10^{12}$	0.019	0.14
6	$1.3 \cdot 10^5$	$1.9 \cdot 10^{13}$	$1.7 \cdot 10^{12}$	$7.9 \cdot 10^{12}$	0.092	0.41
7	$1.2 \cdot 10^5$	$1.7 \cdot 10^{13}$	10^{13}	$4 \cdot 10^{12}$	0.59	0.23
8	10^5	$1.4 \cdot 10^{13}$	$1.1 \cdot 10^{12}$	$3.6 \cdot 10^{12}$	0.078	0.26
9	$2.1 \cdot 10^5$	$3 \cdot 10^{13}$	$8.5 \cdot 10^{11}$	$3.6 \cdot 10^{12}$	0.028	0.12

for 5 cm < r < 40 cm, and $\rho(r) \sim 1/r$ for 40 cm < r < 80 cm. The lateral distribution of the energy flux obtained for these cases from the first row of ionization chambers was close to $1/r^2$, which is in agreement with the lateral distribution of particle densities going as $1/r$.

The angular distribution of shower particles and the direction of the particle flux near the shower axis was found for one case by means of the diffusion chamber. The angular distribution with respect to the direction of the axis in this event is shown in Table I. The direction of tracks (ϑ, φ) was determined with an accuracy of 1°. The direction of the axis (ϑ^0, φ^0) was taken as a direction of the particle flux in the region of the axis. The method of the determination of the axis region has been described above. With an accuracy up to 1°, the directions of the trajectories of these particles were identical. The angle with respect to the shower axis θ^* was determined from the usual formula

$$\cos\theta^* = \sin\vartheta^0 \sin\vartheta \cos(\varphi^0 - \varphi) + \cos\vartheta^0 \cos\vartheta.$$

Therefore, the accuracy of the determination of the direction of single trajectories amounted to 2°.

It can be seen that the angular distribution in the shower core is rather broad and the contribution of large angles increases substantially with increasing r (see Table I). A problem arises, therefore, as to the accuracy with which the direction of the particle flux at a certain distance from the shower axis reflects the direction of the axis. In view of the very broad angular distribution of shower particles, we cannot find a vector of a mean direction for the given shower with sufficient accuracy to maintain that it is parallel to the shower axis. Thus, at a distance of about half a meter, the formally determined mean direction forms an angle of ~ 5° with the axis.

We shall mention briefly the data on the nuclear-active component. If the position of the axis is known from the first row of ionization chambers, and its direction from the diffusion chamber with an accuracy to 5°, then we can find the position of the axis from the second row of chambers and study the presence of high-energy nuclear-active particles in the immediate vicinity of the shower axis. Data on the energy flux of the nuclear-active and electron-photon component around the shower axis in a circle of radius 1 m are given in Table II. The energy of the nuclear-active component was determined from the size of the burst in the second row of chambers in the same way as in reference 8. Table II (last column) shows that the ratio of the energy carried by the electron-photon component of the core to the total energy of the electron-photon component in the shower has a large spread.

It can also be seen from Table II, where a part of the mentioned 28 events is discussed, that showers with the same total number of shower particles can have a substantially different amount of high-energy nuclear-active particles in the core and, correspondingly a different total energy of these particles in the core. In a number of events, around the point of intersection of the shower axis or in the prolongation of the axis, one observes one high-energy nuclear-active particle carrying the main fraction of the energy of the selected region near the axis. In a number of cases, the energy is carried by several nuclear-active particles of smaller energies. Therefore, the array makes it possible to study the structure of the core of high-energy showers in sufficient detail. This is not the case for the study of cores of EAS of small energies.

In the case of low energy showers, the density of particle flux near the axis may be insufficient for any accurate location of the axis. It is even more important that, in showers of low density, the nuclear cascade consists of particles of lower energies which suffer a more marked angular spread. It is evident that a marked deviation will also be suffered by π^0 mesons which start the electron-photon cascade, a fact which can cause an ambiguity in the axis location. Therefore, for the core and position of the axis of an individual

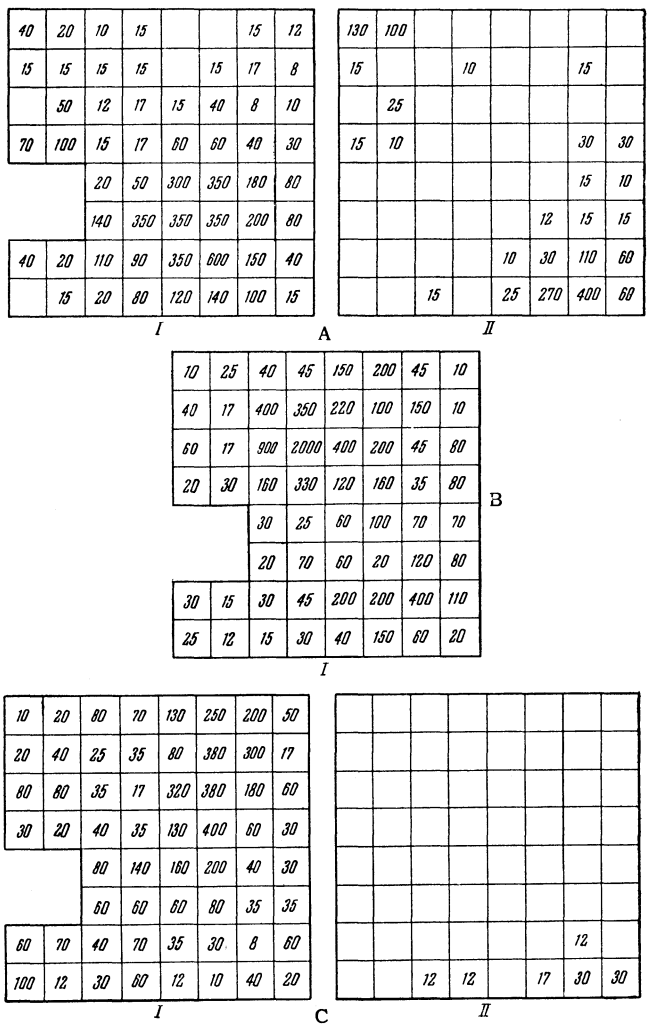

FIG. 7. Distribution of ionization expressed as the number of relativistic particles passing through a chamber in the first row of ionization chamber (I), and in the second row of ionization chambers (II). A – passage of the core of a shower with $N = 10^4$, lateral distribution of energy flow first row $\sim 1/r^2$; B – passage of a core of a shower with the total number of particles $N = 10^4$, lateral distribution of energy flux (first row) $\sim 1/r^2$. No ionization in the second row of ionization chambers (or smaller than the value of the amplifier noise); C – passage of a core of a shower with a total number of particles $N = 2 \times 10^4$, lateral distribution of energy flux (first row) $\sim 1/r$.

shower have no meaning, and the showers can be studied only statistically. In connection with this, we have limited ourselves in the study of low energy showers to EAS of medium size with a number of particles in the range of $2 \times 10^4 - 6 \times 10^4$.

During the operation time of the array (1000 hours), we found 40 events where the axis of such showers fell on the area of the first row of ionization chambers. This number is in good agreement with the one expected according to reference 6. Examples of observed cases are shown in Fig. 7.

All events correspond to the presence of a sufficiently sharp gradient and a region with maximum density of particles. Lateral distribution of energy flux suffers large fluctuations from $1/r$ to $\rho(r)$ close to $1/r^3$ for 30 cm < r < 1 m, and the events with the given $\rho(r)$ are found approximately as frequently as for showers of higher energies discussed above.

0	0	0	0	0	0	0	0	0	0	0
0	0	2	0	2	0	0	1	1	2	0
1	0	0	0	0	1	1	1	0	1	1
0	0	0	0	0	1	1	1	2	0	1
0	0	0	1	0	0	1	0	1	1	2
0	1	0	0	1	4	2	1	2	0	1
0	1	0	0	2	0	2	2	1	1	1
0	0	1	0	2	0	9	6	3	1	0
1	0	0	0	1	3	15	35	6	0	1
1	0	1	1	1	3	2	10	1	1	1
1	0	1	0	0	1	0	2	0	3	1

FIG. 8. Distribution of the flux of shower particles in the diffusion chamber accompanying the passage of an axis of an EAS with $N = 3.5 \times 10^4$ through the chamber.

It should be noted that, in a number of cases at a certain distance from the axis, we observed local increases in particle density connected with the fact that high-energy electrons and photons deviate from the shower axis. These increases in density are more noticeable in showers of medium size than in showers of large size, since the axis region in the first group is less rich in energy. However, in the showers discussed above, the energy density of the electron-photon component near the axis is still sufficiently high to localize the axis with an accuracy up to the dimensions of the chamber. This is not the case in a number of events where the axis is located in the diffusion chamber and where the particle density flux, and not the energy flux, is measured. Out of 40 cases of incidence of axis on the first row of ionization chambers, in six events the axis fell on the part of the row which is placed above the diffusion chamber. One of these is shown in Fig. 8. It can be seen that the particle density is so low that it can be distinguished from the background only at distances not greater than 20 – 30 cm from the axis. In a number of events, the axis may be localized satisfactorily even without the data from the first row of ionization chambers. In a number of events, these data are absolutely necessary in view of the small flux of particles. In the first case, there is a sharp increase in density near the axis, from $1/r$ to $1/r^{1.5}$ in the range from 40 to 5 cm while, in the second case, the increase is slower, or even non-existent. The energy fluxes carried by the

nuclear-active component of the core of the observed shower also fluctuate. These fluctuations, however, can be partly due to a possible deviation of nuclear-active particles forming the nuclear cascade from the axis of the electron-photon shower at distances bigger than the size of the array, and also due to fluctuations in the fraction of the energy transferred to π^0 mesons in nuclear interactions in the layer of graphite.

The study of the cores of individual showers at sea-level, by means of the method described above, therefore showed the following phenomena:

1. For EAS with a number of particles $> 10^5$ in the core of the shower ($r < 1$ m) nuclear-active particles are observed, the total energy of which is on the average, of the order of the energy of the electron-photon component at the same distances from the axis. However, in individual showers, the magnitude of the ratio of the energy of the nuclear-active component ot the energy of the electron-photon component can have different values.

2. The density of the energy flux carried by electron-photon component of EAS in showers with $N \geq 10^5$ particles shows a marked increase down to 30 cm from the axis (for the majority of showers). The dependence of the density of the energy flux of the electron-photon component on the distance from the axis of the shower cannot be expressed by a general function for all showers. From the found cores in the distance range of $30 - 100$ cm from the axis, the decrease of the energy flux density with distance varies from $1/r$ to $1/r^3$.

3. The energy of the electron-photon component of showers contained in the core region of the shower ($r < 1$ m), normalized to the number of particles in the shower, has a big spread, and can vary from shower to shower by a factor of up to 10.

4. The energy of the nuclear-active component in showers with $N > 10^5$ also has no non-ambiguous correspondence with the number of particles in the shower, and suffers a large spread.

The authors would like to express their deep gratitude to Academician D. V. Skobel'tsyn for his great help in the work and his constant interest; to V. V. Borisoglebsky for constant help; to Prof. N. A. Dobrotin for his help and discussion of results; and also to the group of co-workers on the array for the study of EAS in Moscow State University: A. T. Abrosimov, S. S. Glagolevskiĭ, B. V. Subotin, A. D. Erlykin, A. B. Kamnev, and E. N. Sosnovets who helped in carrying out the experiments.

[1] Vavilov, Nikol'skiĭ, and Tukish, Dokl. Akad. Nauk SSSR **93**, 233 (1953).

[2] Abrosimov, Bedniakov, Zatsepin, Nechin, Solov'eva, Khristiansen, and Chikin, J. Exptl. Theoret. Phys. (U.S.S.R.) **29**, 693 (1955), Soviet Phys. JETP **2**, 357 (1956).

[3] Dobrotin, Zatsepin, Nikol'skiĭ, Sarycheva, and Khristiansen, J. Exptl. Theoret. Phys. (U.S.S.R.) **19**, 666 (1955).

[4] Abrosimov, Goriunov, Dmitriev, Solov'eva, Khrenov, and Khristiansen, J. Exptl. Theoret. Phys. (U.S.S.R.) **34**, 1077 (1958), Soviet Phys. JETP **7**, 746 (1958).

[5] G. T. Zatsepin, The Oxford Conference on EAS, Harwell, 1956.

[6] G. V. Kulikov and G. B. Khristiansen, J. Exptl. Theoret. Phys. (U.S.S.R.) **35**, 635 (1958), Soviet Phys. JETP **8**, 441 (1959).

[7] Anishenko, Zatsepin, Rosental, and Sarycheva, J. Exptl. Theoret. Phys. (U.S.S.R.) **22**, 143 (1952).

[8] Dmitriev, Kulikov, and Khristiansen, Suppl. Nuovo cimento (in press).

[9] Abrosimov, Dmitriev, Massal'skiĭ, Kulikov, and Khristiansen, J. Exptl. Theoret. Phys. (U.S.R.R.) **36**, 751 (1959); Soviet Phys. JETP, this issue, p. 000.

[10] I. P. Ivanenko, Dokl. Akad. Nauk SSSR **107**, 819 (1956), Soviet Phys. "Doklady" **1**, 231 (1956). J. Exptl. Theoret. Phys. (U.S.S.R.) **31**, 86 (1956), Soviet Phys. JETP **4**, 115 (1957).

[11] N. N. Goryunov and A. D. Erlykin, Приборы и техника эксперимента (Instruments and Meas. Engg.) No. 1 (1959) (in press).

[12] N. N. Goryunov, Приборы и техника эксперимента (Instr. and Meas. Engg.) No. 3 (1959) (in press).

Translated by H. Kasha
127